

Detailed Waveform Inversion for Moment Tensors of $M \sim 4$ Events: Examples from the Corinth Gulf, Greece

by Jiri Zahradnik, Jaromir Jansky, and Vladimir Plicka

Abstract Moment tensors (MTs) of weak events are often calculated by a single agency (network), thus lacking independent validation. This article investigates how to increase reliability of the single-agency solutions through various multiple checks. It deals with the inversion of complete waveforms for six representative events (M_w 3.4–4.6) in the range of 0.08–0.15 Hz. Several three-station sets at near-regional distances (8–103 km) are used. The MTs are repeatedly calculated for two independent locations: from a regional and local network. The source depth is held fixed at the hypocenter and also grid searched to optimize the waveform match. Initially, large variations (instability) of the MT solution with the approach we used were found for some events. Later, the difficulties were understood and the solutions stabilized. It led to practical recommendations on how to detect or even avoid problematic MT solutions. First, avoid MT solutions for a single fixed depth (hypocenter). Second, optimize MT solutions by the depth grid search below epicenter (or better) for at least two alternative epicenters. Third, carefully analyze: (i) any rapid variation of the solution, (ii) major misfit of the first-motion polarities, (iii) low double-couple percentage (often correlating with [ii]), (iv) low values of the min / max eigenvalue ratio, and (v) departures of the MT-preferred depth from the location-derived depth. The MT-preferred depths, hence also the focal mechanism, may be misleading due to data problems (e.g., long-period disturbances, clipping) hidden in the band-pass waveforms. The location-derived depth may be especially wrong for very shallow earthquakes if the crustal model is inadequate in its shallow part and/or near stations are lacking. On the other hand, near stations (<20 km) should not be used in the waveform inversion together with distant stations; because of their large amplitudes, the inversion can be easily biased due to instrumental data errors and small location errors.

Online Material: Color figures and waveform match.

Introduction

Moment tensors (MTs) represent key information for seismotectonic studies. A powerful tool for the MT calculation is the waveform inversion. Many agencies report MTs down to relatively weak events (e.g., $M_w > 4.5$ for the European-Mediterranean region and $M_w > 3$ in the Alpine region; Braunmiller *et al.*, 2002; Pondrelli *et al.* 2006). Nevertheless, critical evaluation of methodical limitations is still rare (e.g., Jost *et al.*, 2002; Richardson and Jordan, 2002; Tajima *et al.*, 2002; Bernardi *et al.*, 2004; Clinton *et al.*, 2006; Sileny and Milev, 2006; Templeton and Dreger, 2006). Moreover, with the increasing number of new broadband networks, not all operators are aware of potential pitfalls, in particular, when trying to get at $M \sim 4$ and below. It is dangerous because weak events have often just a single-agency solution, lacking an independent validation.

This article aims at better understanding methodical problems of weak events. The goal is to investigate how to increase reliability of a single-agency solution through various multiple checks. The article focuses on the inversion of complete near-regional waveforms and discusses repeated MT inversions for six representative $M \sim 4$ events in the Gulf of Corinth, Greece. A specific feature of this study is that a sparse regional network of broadband (BB) stations is combined with a local short-period (SP) network (Fig. 1). Therefore, the earthquake locations can be considered relatively accurate, and the examples are well suited for discussing effects of various alternative estimates of the source position.

The structure of the article is as follows: first, we qualitatively discuss the factors affecting the MT solutions, such

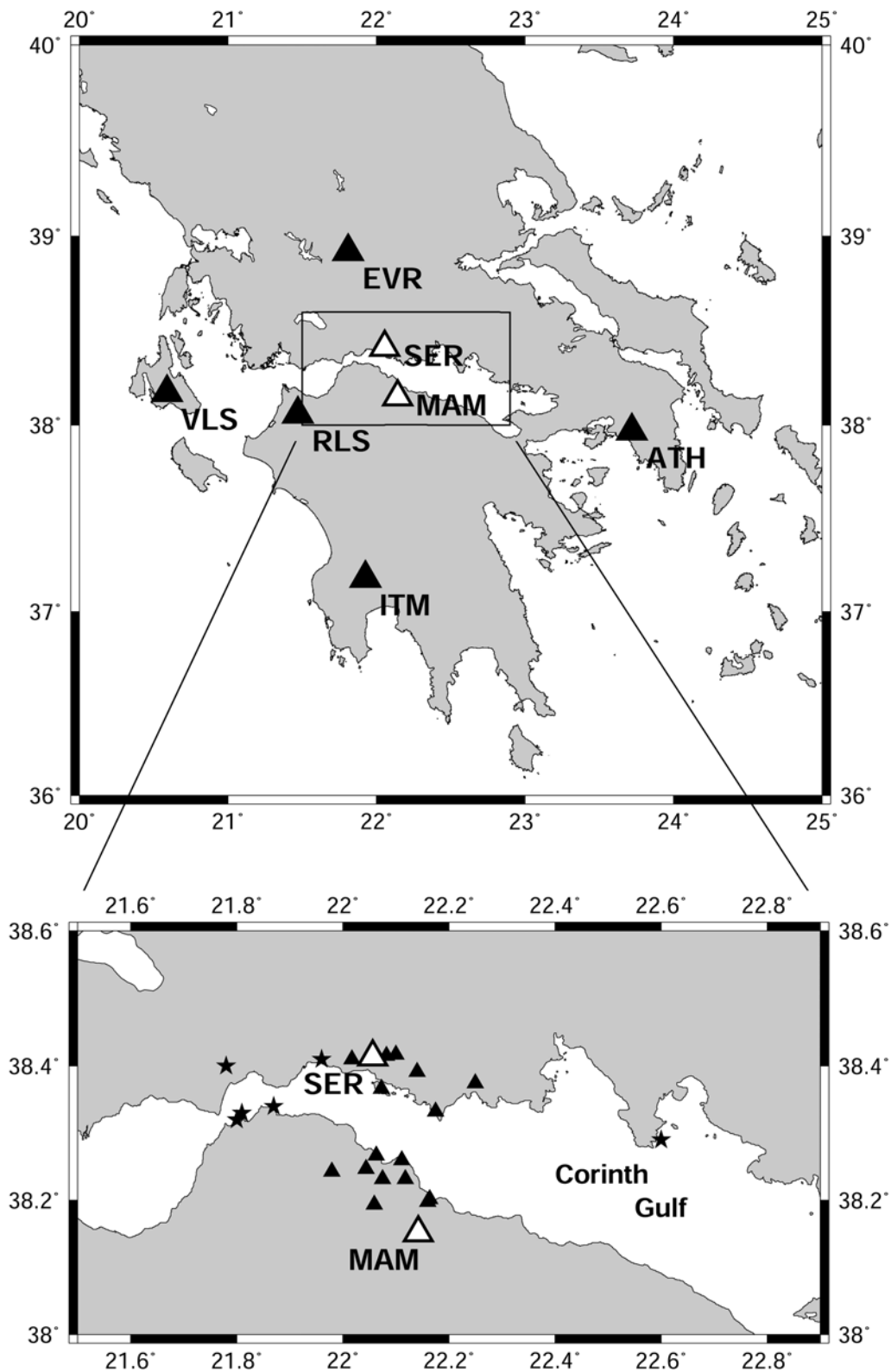


Figure 1. Broadband near-regional stations used in this study (full triangles for NOA and open triangles for Prague–Patras). The inset shows the short-period local network (CRL, small triangles) in the western part of the Corinth Gulf. Epicenters of the studied events are also included (stars). © The color version of this figure is available in the electronic edition of *BSSA*.

as the type of instrument, the quality of the location, the epicentral distance, the crustal model, the frequency range, etc. Next, we select one factor, especially the source position, and quantitatively analyze its effect in four repeated inversions of the selected events. The tests simulate a case where several operators calculate the MT of the same events and obtain generally unequal results due to various adopted strategies. Four more (revised) tests are performed for problematic events with the intention to stabilize their solutions. Finally, an attempt is made to formulate recommendations on how to detect and avoid problematic MT solutions.

Qualitative Analysis

Moment Tensor

Waveforms are related to the source and medium properties by means of the MT and the Green's tensor. Assuming knowledge of the Earth's elastic structure, as well as position of the source and station, synthetic Green's functions can be calculated. When considering regional stations dominated by interference crustal phases, full (= complete) elastodynamic Green's functions must be used. The same is true if the near-field effects are to be analyzed at local stations. In horizontally layered one-dimensional 1D crustal models, the full Green's functions can be calculated basically by any frequency wavenumber or reflectivity method. Then, the MT retrieval is a linear inverse problem, formally overdetermined and solved by the least-squares method. If the source position and time are also to be determined, the least-squares method is complemented by a spatiotemporal grid search.

The full moment tensor has a deviatoric and volumetric part. Retrieval of the volumetric part is very problematic, although not impossible (e.g., Frohlich, 1994; Campus and Faeh, 1997; Dreger and Woods, 2002). Fortunately, the inverse problem remains linear even if limited to the deviatoric moment tensor. The deviatoric tensor can be decomposed into the double-couple (DC) and non-double-couple (non-DC) component. The decomposition is nonunique (e.g., Jost and Hermann, 1989); a very common decomposition is that into the DC and CLVD part, also followed in this article. Here, CLVD stands for the compensated linear vector dipole. The DC and non-DC (= CLVD) parts have relative sizes $(1 - 2f)$ and $(2f)$, respectively, where 1 , $f - 1$, and $-f$ are the normalized MT eigenvalues. The term $100(1 - 2f)$ is referred to as the double-couple percentage, DC%. Usefulness of the non-DC component as a physical parameter of tectonic earthquakes is highly limited due to many masking effects, such as incomplete structural information, sparseness of networks, curvature of faults, source complexity, and anisotropy (Sileny *et al.*, 1996; Julian *et al.*, 1998; Yunga *et al.*, 2005; Roessler *et al.*, 2007; Vavrycuk, 2007). Routine agency reports of the non-DC components are highly variable; stabilized estimates need special techniques on the

scientific rather than on the routine level (e.g., hierarchic grid search or DC versus correlation plots; see Adamova *et al.*, 2008; Zahradnik, Sokos, *et al.*, 2008). On the other hand, low DC% values may be used as a practical, useful, technical tool to detect defects of the models used. Alternatively, a large DC% may be imposed as a soft constraint (e.g., Dreger and Savage, 1999; Cesca *et al.*, 2006).

The size of the deviatoric moment tensor and orientation of its eigenvectors are relatively stable. They can be characterized by the scalar moment, strike, dip, and rake. As a rule, these parameters coming from the deviatoric inversion are close to those from the so-called DC-constrained inversion (Henry *et al.*, 2002), but nonlinearity of this constraint is an unnecessary complication in practice. Therefore, on the routine level of the network operation, calculation of the deviatoric MT is reasonable but users (e.g., geologists) should be aware that usually only the scalar moment, strike, dip, and rake are robust.

Specifically, this article calculates the deviatoric MT and mainly analyzes these four robust parameters. We also calculate the DC% for all inversions, but we point out only cases with $DC\% < 50$, assuming them to indicate a problematic model.

The computer code ISOLA is used (see the Data and Resources section), combining the computational speed of Fortran and the users' comfort of Matlab (Sokos and Zahradnik, 2008). It makes use of the inverse-problem formulation of Kikuchi and Kanamori (1991), based on six elementary MTs. Their equation (6) is used to quickly evaluate the correlation between observed and synthetic waveforms. The Green's functions are calculated by the discrete-wavenumber method (Coutant, 1990; Bouchon, 2003). The match between the observed and best-fitting synthetic data is characterized by the overall variance reduction: $\text{varred} = 1 - E/O$, where $E = \sum(O_i - S_i)^2$, $O = \sum(O_i)^2$, with O and S standing for the observed and synthetic data, along with summation over all samples, components, and stations. The code also allows complex rupture histories described by multiple point-source subevents, each one represented by a delta function (Zahradnik *et al.*, 2005).

The least-squares equations are characterized by eigenvectors and eigenvalues of the corresponding matrix (avoid confusion with the MT eigenvalues). Small eigenvalues indicate that the matrix is close to singularity, hence the MT inversion becomes ill conditioned. What is small and what is large depends on the problem under study. Therefore, we introduce a ratio of the minimum and maximum (absolute valued) eigenvalues, denoted as the min/max eigenvalue ratio, and, based on experiments, we set up a threshold of 0.1. The min/max ratio values below 0.1 are considered close to an ill-conditioned case. They will be denoted by the E symbol. The ratio depends on the event-stations configuration and the structural model, not on the waveform data.

Crustal Model, Epicentral Distances, Frequency Range, Instruments

With current knowledge of the crustal structure, waveforms can be deterministically modeled at only low frequencies, specified in the following, but their availability for weak events at near-regional epicentral distances (< 300 km) is limited by natural noise. Thus, $M \sim 4$ waveforms can be investigated at a limited distance range and limited frequency range. As such, the number of usable stations is usually small (e.g., 5, not 50). Fortunately, compared to MT calculations from amplitudes or amplitude ratios (Jechumtalova and Sileny, 2005), very few waveforms seem to often provide relevant focal mechanisms (e.g., three stations or, for particular event-station geometries, even fewer) (Campus *et al.*, 1996; Dreger and Savage, 1999).

On one hand, the restriction to relatively small epicentral distances and low frequencies is an advantage: the waveforms are less dependent on the crustal model. Synthetic seismograms calculated for several models available for the region under study often provide almost identical waveforms.

On the other hand, small epicentral distances also carry difficulties. Indeed, at close stations, long-period disturbances can appear for reasons not yet well understood but likely due to vibration-provoked local tilts. The disturbances can often be removed by numerical modeling (Zahradnik and Plesinger, 2005). Moreover, sensitive weak-motion instruments (e.g., CMG-3T) are also often clipped by $M \sim 4$ at distances of a few kilometers. The latter is solved when accompanying the weak-motion broadband instruments with strong-motion accelerometers, but the higher self-noise of the accelerometers is also a limiting factor of the low-frequency studies of weak events (Zahradnik, 2004).

Specifically for this article, preliminary tests (see an example in the next section) have shown that the low-frequency waveform inversion of $M \sim 4$ earthquakes in the Corinth Gulf should be performed at frequencies higher than 0.08 Hz and preferably at epicentral distances up to 100 km. At lower frequencies and larger near-regional distances, the signal-to-noise ratio (S/N) is poor. The tests with several crustal models of the region (see later) show that at distances up to 100 km, the particular model choice has an insignificant effect upon the waveform match for frequencies near 0.1 Hz. At the same time, none of the available models allows investigation of the frequencies above ~ 0.2 Hz, because in that range, the models already miss the necessary detail of the crustal structure. As such, the allowed distance and frequency ranges are, unfortunately, quite narrow. The disadvantage of a narrow range is obvious: it reduces data and increases vulnerability to noise.

Even small events may have complex rupture histories. However, their correct retrieval may be obscured by possible unmodeled structural effects (Campus *et al.*, 1996). An advantage is that the actual source time function does not need to be investigated, that is, below corner frequency it can sim-

ply be approximated by a delta function, which significantly contributes to the robustness of the method.

Source Position

The MT calculations need an estimate of the source position. We distinguish between hypocenter (provided by the earthquake location procedure) and centroid. Centroid represents the center of gravity of the faulted area. The centroid can be determined during the MT retrieval as a point optimizing the waveform fit, found by grid search around an assumed position. Analogously, a temporal grid search provides the centroid time. For large events, the hypocenter and centroid do not coincide with each other. For $M \sim 4$ events, the hypocenter-centroid distance is comparable, or even smaller, than their errors. For instance, the fault length is ~ 1 km using the empirical relations of Somerville *et al.* (1999). For small events, the centroid can thus be considered equivalent to the hypocenter position, and vice versa. Actually, the situation is more complicated. For a typical regional network with interstation distances of the order of 100 km, the number of stations with satisfactory S/N ratios to locate an $M \sim 4$ event is usually small (e.g., 10 stations). It means that the epicenter position could have errors of the order of 10 km (and of ~ 1 km only if a local network is available). Accurate determination of the depth is even more problematic, because it depends on the availability of a near station with P and S readings. On the other hand, the centroid position is also not exact, because long waves have limited spatial resolution. Then a legitimate question is whether for $M \sim 4$ events the MT calculations should be performed for the hypocenter position, the centroid position, or both or whether and how the varied source position may improve the MT reliability.

Therefore, in the following section, variations of the source position are studied. This is a common approach, but we try to go into more detail. We employ both epicenters from a regional and a local network. We allow vertical variations below the epicenter or we allow the source position to coincide with the hypocenter.

Quantitative Analysis: Data

BB Stations

Waveforms analyzed in this article were initially taken from seven regional BB stations (Fig. 1; see also the Data and Resources section). The BB stations are of two types: (i) five stations of the telemetered network of the National Observatory of Athens (NOA) (Melis and Kostantinou, 2006), equipped with Lennartz 20 sec instruments Le-3D/20s and (ii) two stand-alone stations of the Patras–Prague project (Zahradnik *et al.*, 2005) with collocated force-balance Guralp CMG-3T broadband weak-motion 100 sec velocity meters and CMG-5T strong-motion (SM) accelerometers. The latter were used when the weak-motion records were clipped. Long-period disturbances at near weak-motion BB stations

were removed from records analyzed in this article by numerical modeling (Zahradnik and Plesinger, 2005; Cervinkova, 2006). The first-motion polarities were read from all BB records, paying close attention to the consistency of the three components (to avoid erroneous orientation of the sensor and/or problematic azimuths).

SP Stations

The manual readings of the *P* and *S* arrival times were taken from the database of the short-period three-component network of the Corinth Rift Laboratory (CRL) (Lyon-Caen *et al.*, 2004). The 16-station CRL network is shown in the inset of Figure 1. The first-motion polarities were also read from the *SP* stations (see also the Data and Resources section).

Selected Events

Six events have been chosen for this study to cover the variety of weak earthquakes in the Gulf regarding their position, depth, magnitude, data availability, etc. (Table 1). Event 2 is the weakest ($M \sim 3.5$), and Event 6 is the largest ($M \sim 4.5$) and deepest (~ 80 km). Compared to frequent shallow and mostly normal faulting events in the Corinth Gulf, the intermediate-depth earthquakes, such as Event 6, are much less frequent there; they are attributed to the Hellenic subduction under the Peloponnesos (Benetatos *et al.*, 2004).

Hypocenters

Regional and local hypocenter determinations are distinguished in this article based on different stations and different crustal models. The regional location, determined by the so-called Hellenic network, was taken from the catalog of NOA. The location specifically made in this study using a local network is based on the *P*- and *S*-wave arrival times of CRL and the crustal model of Rigo *et al.* (1996) (hereafter model *R*, see Table 2). For simplicity, it is hereafter referred to as the CRL location. Use of the NOA location is to illustrate a frequent case that the operator calculating a quick MT estimate relies on the available earthquake location performed

by another expert, often in a sparse network of interstation distances on the order of a hundred kilometers. The CRL location, based on accurate readings and a local network, is assumed to represent a more accurate estimate. Of course, its accuracy is also limited because the studied events are outside of the CRL network.

Preliminary Tests

Without details of focal mechanisms and synthetics, we look at the observed and synthetic displacements of one event (Event 1) to illustrate the noise issue. Figure 2 shows the case of a relatively broad frequency range: 0.02–0.15 Hz. Strong long-period noise is present, mainly at the more distant stations VLS, ITM, and ATH (100–172 km).

Figure 3 shows the same event in the range of 0.08–0.15 Hz, much less disturbed by the noise. We will consistently use this range in the following parts of this article. Tests with 0.08–0.10 Hz gave analogous results; decreasing frequency has a generally positive, stabilizing effect upon MTs, but narrowing the inversion band may have negative effects. For example, the resulting MT might have an erroneous interchange of the *P* and *T* axes. Synthetic waveforms in Figure 3 were calculated in two crustal models: model *R* (Rigo *et al.*, 1996) and model *N* (Novotny *et al.*, 2001), respectively, featuring quite large structural differences, mainly in their shallow parts (Fig. 4). Nevertheless, at distances below 100 km (stations SER, RLS, and EVR where the *S/N* ratio is best), the two crustal models produce almost identical waveforms. Analogous results also hold for other available models of the region (Tselentis *et al.*, 1996; Haslinger *et al.*, 1999). Hereafter, records from VLS, ITM, and ATH are only used for the polarity check, but not for the waveform inversion.

Details of the Inversion

Before MT inversion, the BB (velocity) records are integrated once, and the SM (acceleration) records are integrated twice, in the frequency band of 0.08–0.15 Hz. Complete three-component waveforms are employed without separation of specific wave groups (e.g., *P*, *S*, or *Lg*); these were

Table 1
Earthquakes Selected for This Study

Event Number	Date (yyyy/mm/dd)	Origin Time (UTC) [*]	Magnitude [†]	Stations Used and their Epicentral Distance (km) [‡]
1	2001/12/24	20:55:45	4.4	SER (24), RLS (47), EVR (57)
2	2002/12/03	23:04:39	3.2	SER (18), MAM (32), RLS (47)
3	2003/10/31	02:33:11	4.0	SER (23), MAM (35), EVR (65)
4	2003/11/18	18:32:16	4.1	SER (8), MAM (33), RLS (58), EVR (58) [§]
5	2004/04/28	07:26:58	4.1	SER (25), RLS (41), EVR (66)
6	2005/05/29	08:55:36	4.4	SER (49), RLS (103), EVR (98)

^{*}Approximate origin time (to identify the events).

[†]Local magnitude by NOA-IG.

[‡]Epicentral distance for the CRL location.

[§]Event 4 processed with two three-station sets: SER, MAM, RLS and MAM, RLS, EVR.

Table 2
Crustal Models Used in This Article

Layer Top (km)	P Velocity (km/sec)	Density (g/cm^3)
Model R after Rigo <i>et al.</i> (1996); the P/S velocity ratio is 1.8		
0.0	4.8	2.7
4.0	5.2	2.7
7.2	5.8	2.9
8.2	6.1	2.9
10.4	6.3	3.0
15.0	6.5	3.0
30.0	7.0	3.1
Model N after Novotny <i>et al.</i> , 2001; the P/S velocity ratio is 1.78		
0	2.3	2.16
1	4.3	2.56
2	5.5	2.80
5	6.2	2.94
16	6.4	2.98
33	8.3	3.36

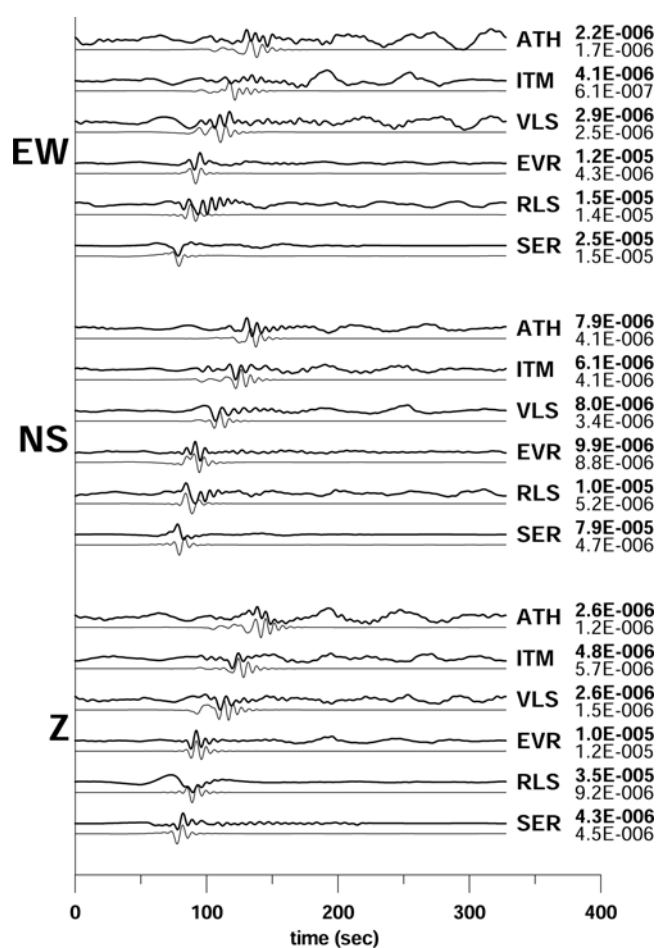


Figure 2. A typical example of the observed (top) and synthetic (bottom) displacements in the frequency range 0.02–0.15 Hz, Event 1. Peak amplitudes (in meters) are on the right-hand side of the figure. The main message of the figure is the prohibitively large low-frequency noise.

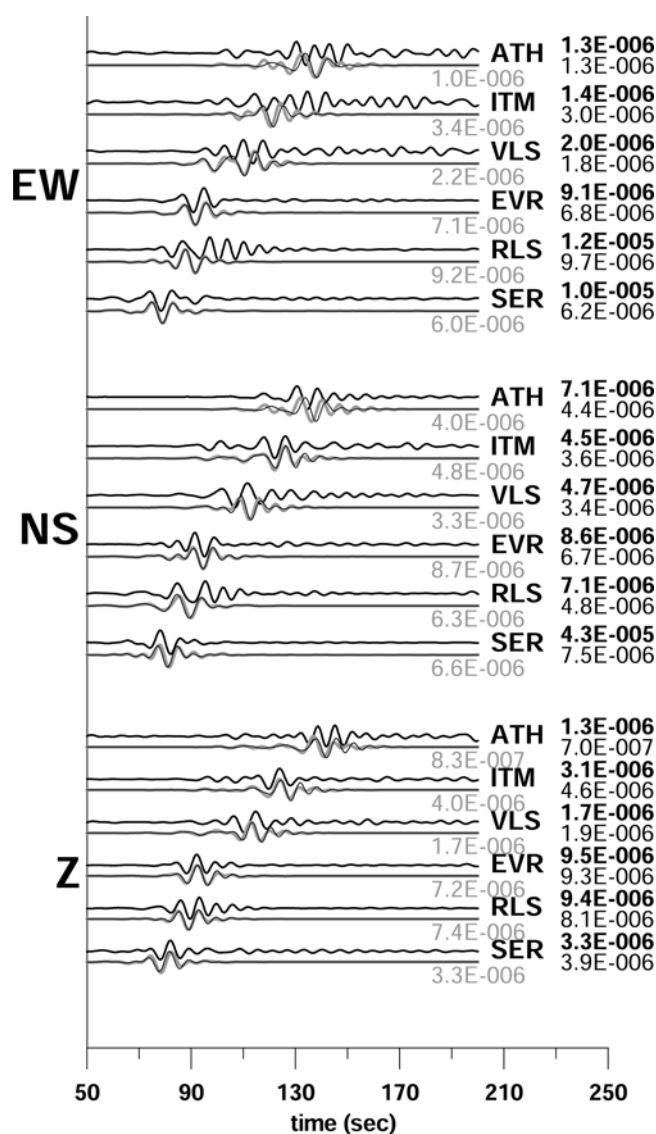


Figure 3. A typical example of the observed (top) and synthetic (bottom) displacements in the frequency range 0.08–0.15 Hz, Event 1. Peak amplitudes (in meters) are on the right-hand side of the figure. The synthetics are calculated for two crustal models: R (solid line) and N (gray line). Note that the effect of the crustal structure is negligible for close stations up to station EVR (66 km) but visible at the more distant stations (107–172 km).

resampled at all stations into 8192 points, with a timestep of 0.04 sec. Waveforms are not shifted to artificially match the first arrival time. The reason is obvious: if the misfit comes from inaccurate location or a local structure at the station, then a simple shift of the whole waveform is not the appropriate correction. The only case where such a shift might be acceptable is the case that the station had grossly wrong timing, say, by a few seconds (e.g., due to technical failure of its global positioning system synchronization). Such a situation can be detected by checking the location P residuals at all stations used for the MT calculation; it is a simple check but is often overlooked in practice. No failure like this was detected in this article.

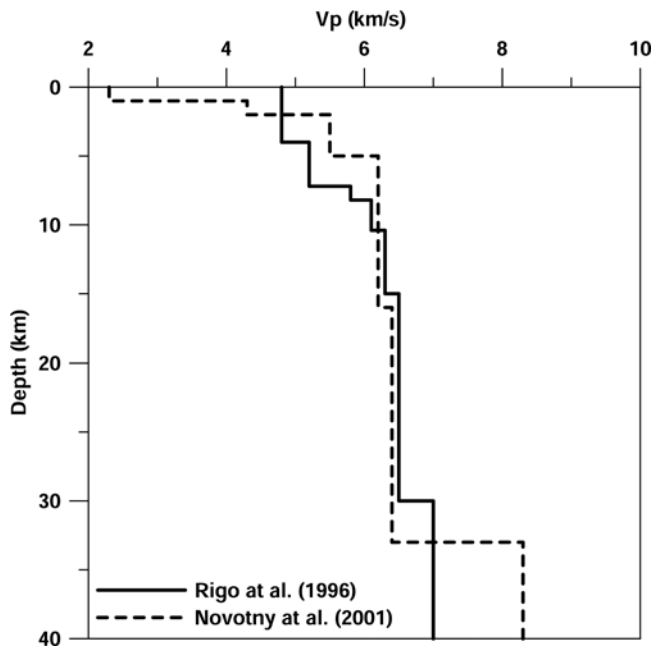


Figure 4. Two crustal models used in this article: *R* (solid line) and *N* (dashed line); see also Table 2.

Records are also not shifted by different amounts of time at individual stations (or components) to improve the match between the observed and synthetic waveforms. The shifts would only be acceptable if they were systematically derived for each source-station pair. Formal shifts are not justified. Moreover, in some cases, tests with intentionally introduced incorrect shifts and incorrect focal mechanisms produced improved matches compared to the correct results. We thus decided against allowing the time shifts. It implies that our inversion results can fully compete with the agency results (often including the shifts), but they might formally look worse because of the lower variance reduction.

The waveform inversion in this article uses the crustal model *R*, the same as the one used for the earthquake location. In a special case (Events 2 and 6), discussed later, the MT solution in model *N* is also needed.

Checking the First-Motion Polarities

We intended to use the same model *R* for also projecting the first-motion polarities on the focal sphere in order to check whether they agree with the MT solution. However, because the model *R* has practically no Moho discontinuity, its mantle velocity being as low as $V_p = 7$ km/sec, we modified the model for the polarity check by adjusting $V_p = 8.3$ km/sec below 30 km. To avoid nonphysical takeoff angles, it is assumed that the first arrivals are direct *P* or *Pn* waves, that is, formal headwaves from intracrustal discontinuities are not allowed (an important detail, although not yet broadly recognized). Even if the polarities look clear, they need a great care for several reasons. At large distances, where the first arrival is *Pn* (in this article, often the case of

ITM, VLS, ATH), the polarity is only used when detecting both *Pn* and *P* on raw seismograms at times predicted by the model. At small distances, problems arise not only from the not-so-well known structure, but also from the location inaccuracy. A kilometeric shift of an epicenter might cause an almost 10° error in the azimuth.

Therefore, the polarity check should be designed in a robust way, only to detect major polarity problems. In this article, a major polarity disagreement is declared (marked by *P* in the column labeled Problem in Table 3) if a station with a clear compression onset is detected in the dilation sector, or vice versa, far from nodal lines. On the other hand, if some observed polarities are not satisfied, but a small adjustment of the calculated solution (e.g., a change of the strike, dip, or rake by a few degrees) brings the calculated and observed polarities in agreement, the MT solution may still be considered satisfactory. This is also why the polarities should be used as a posterior check and not a prior constraint.

The easiest is the diagnosis of the most severe polarity problem: the MT solution providing incorrect sign at all stations and components, when the rake angle is erroneously substituted by rake -180° , characterized by the *P-T*-axes interchange (already mentioned previously).

Quantitative Analysis: Results

Repeated Inversions with Variable Source Position

To facilitate the methodical comparison, each event is solved using a set of three stations (with distances up to ~ 100 km); see Table 1. Four strategies to set up the source position at which the MT is calculated are compared: (a) the source position is held fixed at the hypocenter of the regional (NOA) location. (b) The source position (centroid) is grid searched to optimize the waveform fit below the NOA epicenter. Cases (c) and (d) are analogous, but with the CRL (local network) determination. All four cases include the waveform optimization by a temporal grid search of the source time. This is important because we work with observed waveforms aligned to a (more or less arbitrary) common origin time, unchanged even when the spatial source position is changed. Most calculations (b) and (d) are for depths 2, 4, \dots , 20 km. The exceptions are for Event 2 (0.3, 0.8, \dots , 4.8 km) and Event 6 (50, 55, \dots , 95 km).

The four inversions are presented in sections (a)–(d) of Table 3 and Figures 5 and 6. (See also Figure S1 in the electronic edition of *BSSA*.) The fault-plane solutions (the beach balls) enable a visual comparison with the main intention of detecting a big change when two mechanisms represent a different tectonic style, that is, normal, reverse, or strike slip.

As clearly seen from Figure 5, three of the studied events (Events 3, 5, and 6) have very stable fault-plane solutions, independent of the approach used. Their first-motion polarities are basically correct (there are no *P* symbols in the column labeled Problem in Table 3). It is true even for the

Table 3
The MT Solution of the Studied Events (Table 1) Calculated by Different Approaches

(a) Epicenter from Regional Network (NOA), Hypocenter Depth										
Event Number	Longitude (°E)	Latitude (°N)	Depth (km)	Strike (°)	Dip (°)	Rake (°)	M_w	Variance Reduction	Problem	
1	21.76	38.36	5	239	59	-63	4.2	0.43	DC, <i>P</i>	
1 revision	21.76	38.36	5	100	43	-55	3.9	0.15	DC, <i>P</i>	
2	21.91	38.34	10	150	87	12	3.5	0.39	DC, <i>P</i>	
2 revision	21.91	38.34	10	156	64	35	3.4	0.41	DC, <i>P</i>	
3	21.82	38.33	16	96	80	-35	4.1	0.42		
4	22.00	38.41	13	111	67	-80	4.4	0.52	<i>E</i>	
4 revision	22.00	38.41	13	117	64	-69	4.4	0.46		
5	21.82	38.32	15	90	65	-41	4.2	0.37		
6	22.73	38.26	104	91	33	-163	4.7	0.34	DC, <i>E</i>	
6 revision	22.73	38.26	104	264	28	151	4.7	0.26	DC, <i>P</i> , <i>E</i>	
(b) Epicenter from Regional Network (NOA), MT-Preferred Depth										
1	21.76	38.36	42	71	89	48	4.6	0.64	DC, <i>P</i>	
1 revision	21.76	38.36	10	105	47	-48	4.1	0.20	DC, <i>P</i>	
2	21.91	38.34	0.8	302	54	-59	3.4	0.43	<i>P</i> , <i>E</i>	
2 revision	21.91	38.34	1.3	286	33	-105	3.3	0.49		
3	21.82	38.33	10	96	77	-38	4.0	0.56		
4	22.00	38.41	4	74	89	-95	4.2	0.64	<i>P</i> , <i>E</i>	
4 revision	22.00	38.41	8	106	60	-75	4.3	0.53		
5	21.82	38.32	12	92	67	-38	4.2	0.38		
6	22.73	38.26	75	102	41	-146	4.6	0.48	<i>E</i>	
6 revision	22.73	38.26	60	120	48	-128	4.6	0.40	<i>E</i>	
(c) Epicenter from Local Network (CRL), Hypocenter Depth										
1	21.78	38.40	7	93	83	-10	4.2	0.52		
1 revision	21.78	38.40	7	112	89	-37	4.0	0.43		
2	21.87	38.34	9	151	84	-1	3.4	0.32	DC, <i>P</i>	
2 revision	21.87	38.34	3	140	52	-43	3.3	0.32	<i>P</i>	
3	21.81	38.33	14	96	81	-39	4.1	0.52		
4	21.96	38.41	10	95	65	-99	4.4	0.67	<i>E</i>	
4 revision	21.96	38.41	10	103	64	-93	4.4	0.68		
5	21.80	38.32	16	92	64	-51	4.2	0.38		
6	22.60	38.29	80	95	39	-157	4.6	0.46	<i>E</i>	
6 revision	22.60	38.29	80	117	25	41	4.6	0.31	DC, <i>P</i> , <i>E</i>	
(d) Epicenter from Local Network (CRL), MT-Preferred Depth										
1	21.78	38.40	16	91	85	-12	4.4	0.61		
1 revision	21.78	38.40	10	108	88	-42	4.1	0.46		
2	21.87	38.34	1.3	116	46	-69	3.4	0.41	<i>E</i>	
2 revision	21.87	38.34	2.3	120	46	-65	3.4	0.38		
3	21.81	38.33	8	95	77	-43	4.0	0.60		
4	21.96	38.41	6	79	79	-104	4.3	0.70	<i>P</i> , <i>E</i>	
4 revision	21.96	38.41	6	100	64	-95	4.3	0.73		
5	21.80	38.32	12	91	64	-45	4.2	0.41		
6	22.60	38.29	75	97	41	-154	4.6	0.48	<i>E</i>	
6 revision	22.60	38.29	60	115	45	-137	4.6	0.37	<i>E</i>	

1 revision: excluding NS component at station SER.

2 revision: MT calculations in crustal model *N*.

4 revision: omitting station SER and adding station EVR.

6 revision: MT calculations in crustal model *N*.

M_w is the moment magnitude.

Problems: DC stands for DC percentage below 50%, *P* for major polarity disagreement, and *E* for the min / max eigenvalue ratio below 0.1.

The bold numbers in section (d) denote the most reliable solutions. Only one triplet of the strike, dip, and rake is shown but without claiming that this is the fault plane.

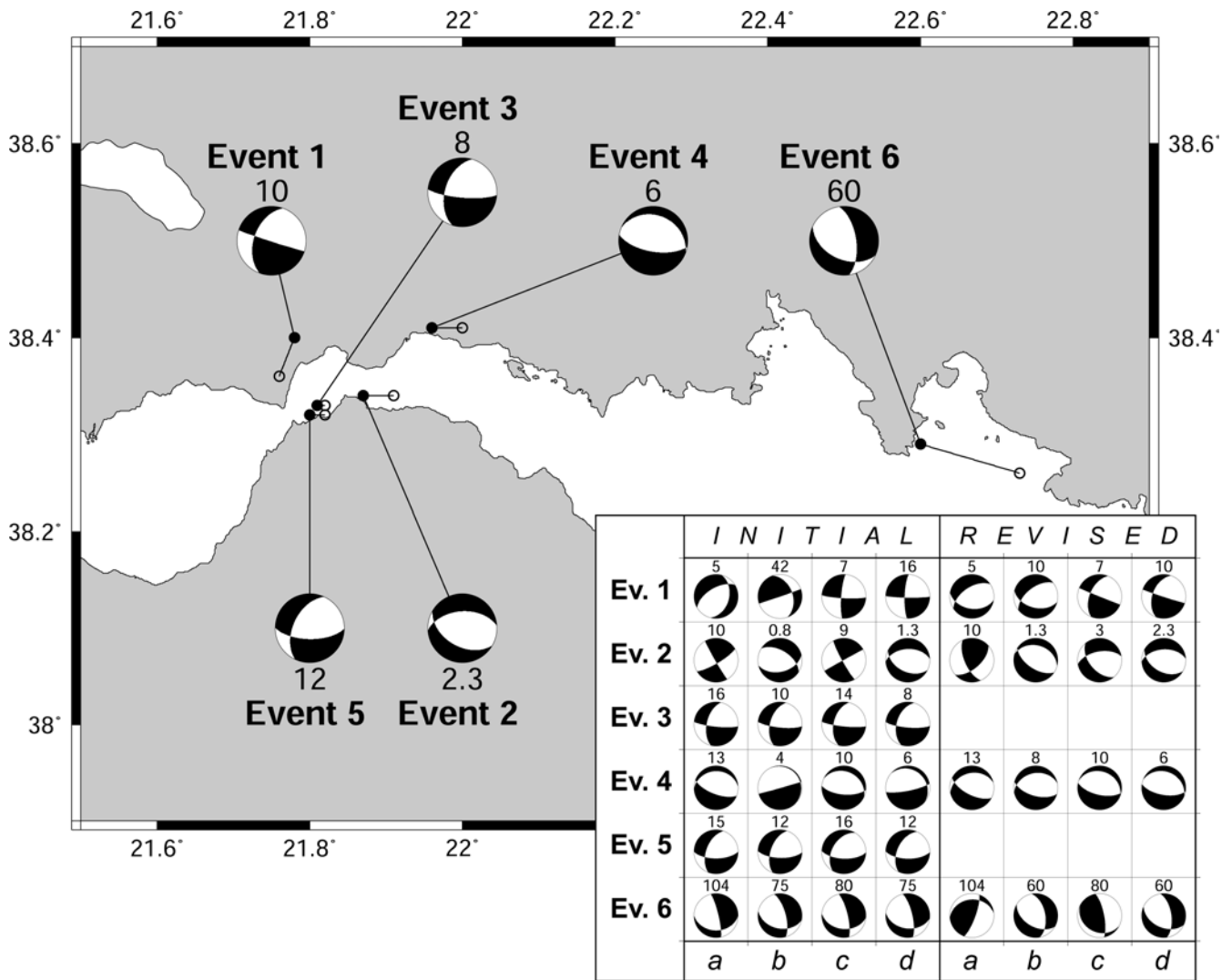


Figure 5. Fault-plane solutions calculated by different approaches (a)–(d) (Table 3). The numbers at the beach balls give the focal depth in kilometers. Note that two events (3 and 5) have a very stable focal mechanism, practically independent of the approach used. The four remaining events are more variable; thus, their revised solutions are also shown. The map demonstrates the two epicenter locations for each event (NOA and CRL, the open and full circle, respectively), connected with each other by a bar. The beach balls in the map correspond to the most reliable solutions, highlighted in section (d) of Table 3. © The color version of this figure is available in the electronic edition of *BSSA*.

MT tensor calculated at the NOA hypocenter position, although its depth differs from the grid-searched optimized depth by as much as 8 km (Event 3). For the deeper Event 6, the depth difference is even larger (104 and 75 km), but practically without any change of the MT solution. Stability of Event 6 is especially interesting (perhaps even puzzling), because the two epicenters that are used differ considerably. This effect comes from the relative simplicity of the waveforms due to the large source depth; synthetic waveforms for different depths in the simple crustal model differ mainly by the time shift; thus, the MT solutions differ practically only in their centroid time.

The fault-plane solutions of the remaining events (mainly Events 1 and 2) vary with the adopted approach, for example, from the normal to the strike-slip type for Event 1. The MT-preferred depths differ very much from the location-

derived depths. Note the extreme depths of 42 km for Event 1 and 0.8 km for Event 2. Relatively close NOA and CRL epicenters yield different MT solutions (Event 1). The CRL epicenter brings correct polarities for Event 1, but it does not hold in the case of Event 2. The variability of the MT solutions among the adopted approaches indicates their possible problems. Therefore, the three events are revised in the following section.

Revision of Event 1

When reinspecting the data, we found that the relatively high value of the variance reduction (0.61 in approach [d]) comes mainly from a good match of the largest north–south (NS) component at the nearest station (SER). If recalculating the variance reduction without that component, it drops down

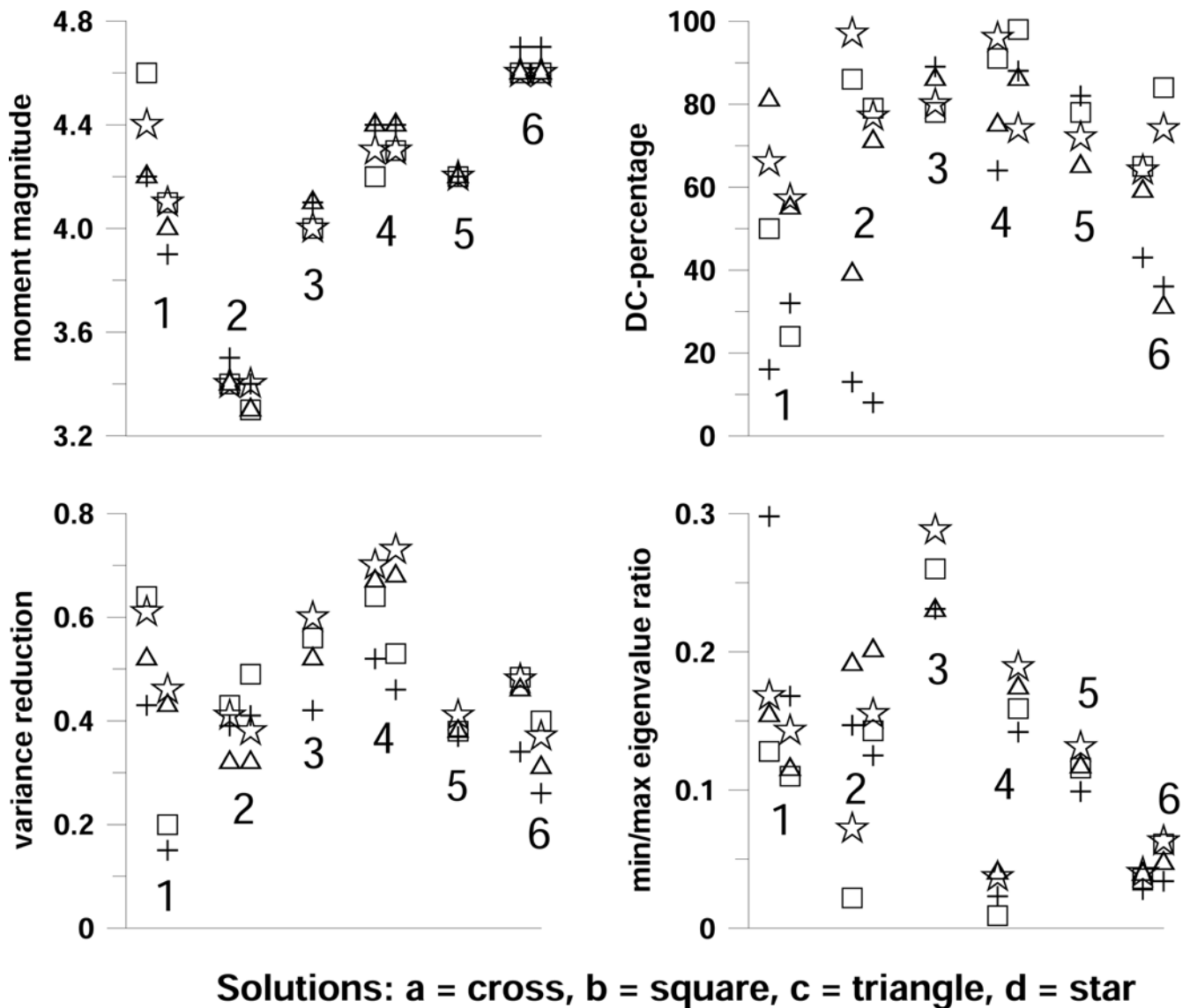


Figure 6. Comparison of all MT solutions of this article (approaches [a]–[d] of Table 3). Note the twin solutions for events 1, 2, 4, and 6, the initial and revised one. Top left: moment magnitude, top right: the double-couple percentage (DC%), bottom left: the overall variance reduction, bottom right: the minimum/maximum eigenvalue ratio of the least-squares equations. © The color version of this figure is available in the electronic edition of *BSSA*.

to 0.1. (Such a check was absent in the initial routine processing.) This means that the SER-NS component biased the inversion. What is the reason? The band-pass displacement (0.08–0.15 Hz) was characterized by an anomalously large amplitude ratio $NS/Z = 14$; see Figure 7. At the same time, the unfiltered raw data had comparable amplitudes on all three components. It indicates a low-frequency problem on the NS component. It most likely resulted from incomplete removal of the long-period disturbance.

Therefore, the revised MT solution for Event 1 is made with omission of the SER-NS component. Again we repeat all four tests, (a)–(d), see Table 3 and Figure 5. As a result, the waveform match improves; see, for example, the shape of SER-Z in Figure 7 and amplitudes of all three components at

EVR; the variance reduction (without SER-NS) increases from the previous value of 0.1 to 0.46. The grid-search depth is now closer to the location depth, and the same is true for the fault-plane solutions at these depths. A small difference remains between the fault-plane solutions for the NOA and CRL locations, but the preferred depth (10 km) is the same.

Revision of Event 2

Event 2 was characterized by a very shallow MT-preferred depth, 0.8 and 1.3 km for the NOA and CRL epicenter position, respectively. The variation of the waveform correlation and the fault-plane solution at the CRL epicenter position is shown as a function of the trial source depth in

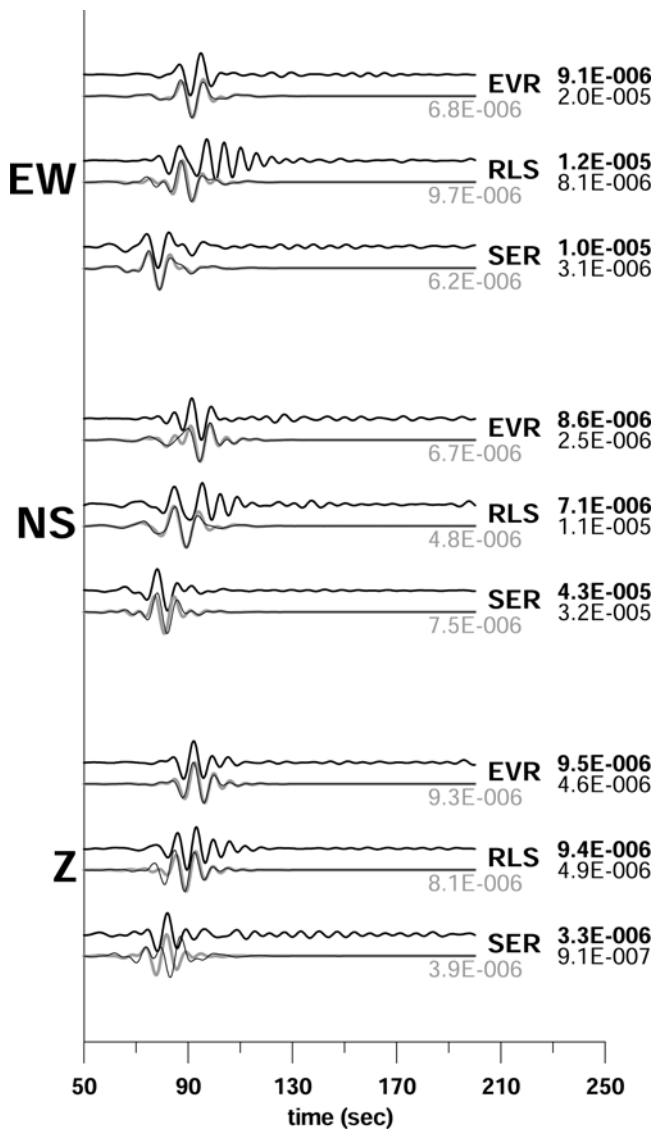


Figure 7. Observed (top) and synthetic (bottom) displacements: Frequency range 0.08–0.15 Hz, Event 1. Peak amplitudes (in meters) are on the right-hand side of the figure. The synthetics are calculated by two approaches, specified in section (d) of Table 3, with all three components at the indicated stations (solid line) and without SER-NS (gray line), respectively. The SER-NS component was wrong and biased the whole inversion. Note the improved waveform fit with the revised solution, for example, in SER-Z.

Figure 8. As seen from this figure, the correlation improvement at the shallow depths (<2.5 km) is quite obvious. Also, the polarities are satisfied at the optimum trial depth of 1.3 km. However, these MT-preferred depths are too shallow in comparison to the hypocenter depths of 9 and 10 km, hence producing large differences between the fixed- and free-depth MTs. Also, the previous seismicity studies of this part of the Corinth Gulf strongly preferred the depths > 5 km (Lattore *et al.*, 2004; Lyon-Caen *et al.*, 2004). The puzzling situation led to a specific study (to be published elsewhere) with a simple conclusion: if an earthquake is very shallow, it is difficult to locate its hypocenter for two reasons. One of

them is an inadequate crustal model, in particular, missing low-velocity layers at the shallow subsurface depths. The other reason is that a correct location of a shallow hypocenter needs a very near station, whose epicentral distance is comparable to the source depth. On the other hand, the MT solution is more robust; it is able to correctly indicate a shallow depth because the relatively low-frequency waveforms are less sensitive to the absence of the low-velocity layers in a simple crustal model as the one used previously (model *R*).

To remove the inconsistency between the MT solution and location of Event 2, we need a better local crustal model in the Corinth Gulf, in particular, at its shallow depths. To at least partially solve the problem, we decided to use the model *N*, just because it contains low-velocity upper layers (Fig. 4) without claiming that it is a preferable local model. Relocating the CRL arrival time data in this model, with an additional station closer to the epicenter, the depth as shallow as 3 km was found acceptable. Therefore, the hypocenter depth of Event 2 was replaced by this value (Table 3, section [c]), and the MT inversion with all four approaches (a)–(d) was repeated with model *N*. The MT-preferred depth below the CRL epicenter is now 2.3 km, the waveform match is comparable to that in model *R* (Fig. 9), and the polarities are also well fit.

As a result, with the relocated hypocenter at the depth of 3 km, the discrepancy between the location and MT-inversion disappears in model *N*. All three approaches (b)–(d) provide very similar fault-plane solutions (see Fig. 5). Naturally, solution (a) still differs remarkably because its fixed depth of 10 km is too far from the MT-preferred depth.

A further investigation of this event would be useful due to its interesting relation to nearby strain measurements. Bernard *et al.* (2006) classified Event 2 as a fast episode of a slow earthquake of equivalent magnitude 5.5, lasting almost two hours.

Revision of Event 4

The initial four tests for this event led to a large difference between the location-derived depth and the MT-preferred depth, similar to Event 1. A problem was detected again in the nearest station SER (now as close to the epicenter as 8 km), but it was not a problem of instrumental origin. At such a small distance, an azimuthal error of about 10° due to uncertainty of the epicenter is possible, having a large effect upon the waveform modeling. The near station is formally fit well with an incorrect mechanism; the remaining stations cannot compensate the problem because their amplitudes (hence implicit weights) are small. Fortunately, another station was available within the 100 km range; thus, the revised MT inversion was performed with addition of the EVR station and omission of SER. As seen in Figure 5, the revised solution is very stable, providing almost the same fault-plane solutions for tests (a)–(d) and resulting in similar MT-preferred depths (not far from the hypocenter depth) for both the NOA and CRL epicenters. Also, the polarities are well fit.

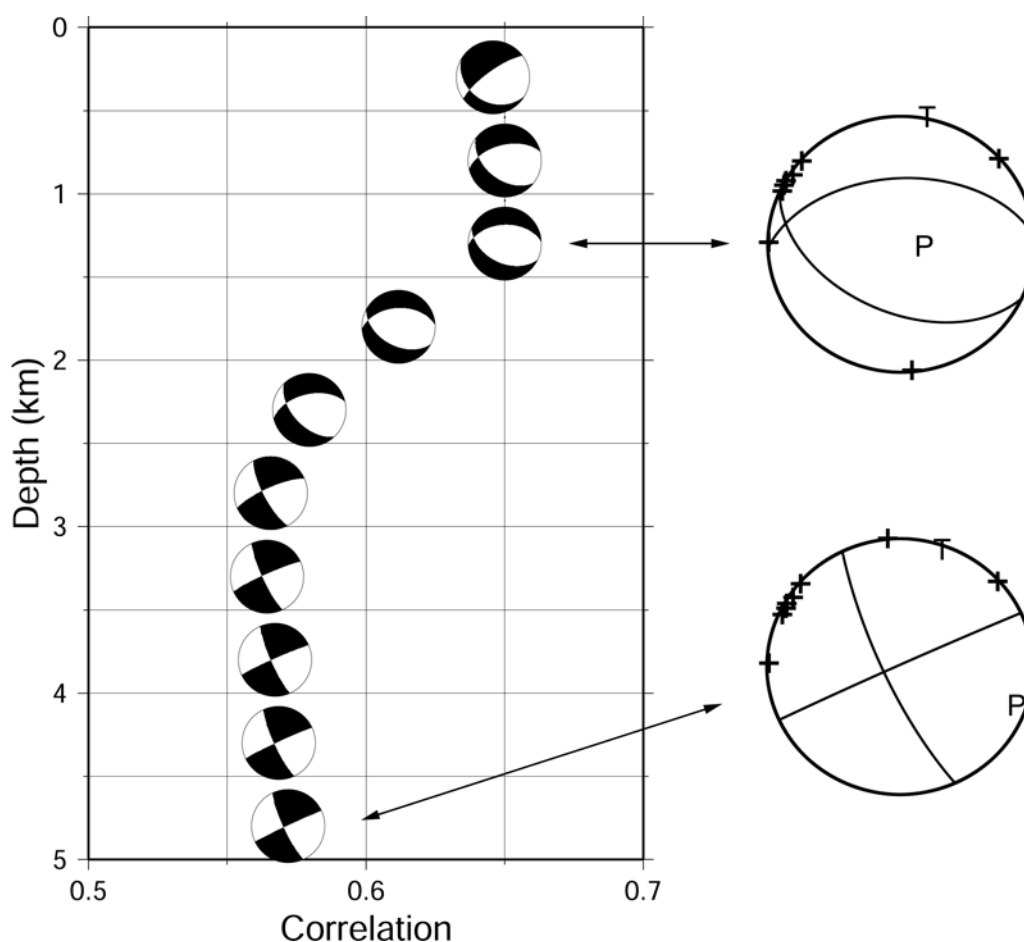


Figure 8. Correlations (between observed and synthetic waveforms) and the fault-plane solutions of Event 2 varying with trial source depth below the CRL epicenter position, model *R*. The shallowest depths are preferred, and just those focal mechanisms are consistent with polarities (all compressions, see inset). Depth 1.3 km: the polarity agreement, depth 4.8 km: the polarity disagreement.

Interestingly, the SER waveform (not inverted) is also fit well, although with a small time shift. (© See Event 4 in Figure S1 of the electronic edition of *BSSA*.)

Revision of Event 6

From Figure 5 and Table 3, it might appear that Event 6 (with its almost identical initial solutions [a]–[d]) does not call for any revision. However, because of its intermediate depth, the event needs more care with regard to the crustal model. Model *R*, formally employed just for easy comparison with the other events, has no Moho discontinuity. Therefore, Event 6 was also revised with model *N* because this model recently proved useful for another intermediate-depth earthquake (Zahradnik, Gallovic, *et al.*, 2008). The well-pronounced Moho in the latter adds more complexity to the solution. As a result, we get a slightly worse waveform match (a lower variance reduction), and, with approaches (a) and (c), we obtain a low DC% and incorrect polarities. In particular, case (c) is characterized by the interchange of the *P* and *T* axes, already mentioned previously. Solutions (b) and (d) with the MT-optimized depth are free of these problems, and their fault-plane solutions are close to those

from model *R* (although 15 to 20 km shallower). Analogously to Event 2, solution (a) differs remarkably, because its fixed depth of 104 km is already too far from the MT-preferred depth. In spite of having the largest magnitude, this event led to a relatively low variance reduction. It might be related to a poor resolution of the moment tensor, indicated by the low min / max eigenvalue ratio. It comes from the relatively short epicentral distances compared to the intermediate depth of this event.

Discussion and Generalization

Comparison

Let us now collectively compare all of the solutions for all six events (Figs. 5 and 6). The main findings can be summarized as follows.

As previously shown, it is possible to detect problematic MT solutions by the following tools:

- Variations of the fault-plane solutions with the used approach,
- Major polarity disagreement between data and synthetics,

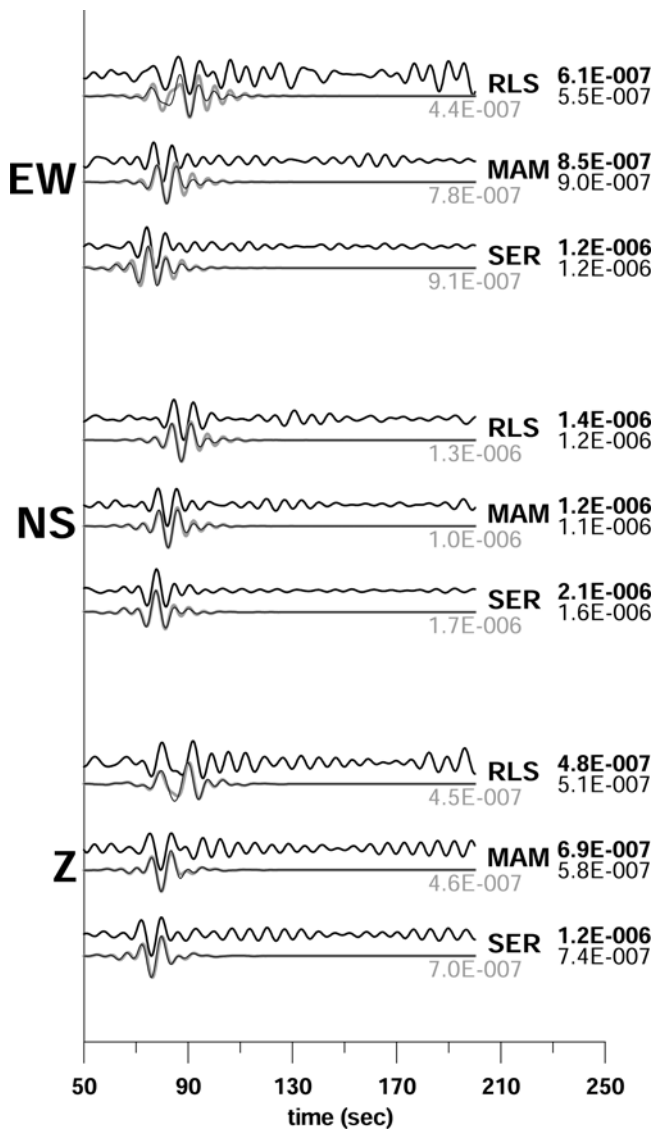


Figure 9. The observed (top) and synthetic (bottom) displacements: frequency range 0.08–0.15 Hz, Event 2. Peak amplitudes (in meters) are on the right-hand side of the figure. The synthetics are calculated in the two very different crustal models of Figure 4: model *R* (solid line) and model *N* (gray line), respectively. Both waveform inversions suggested a very shallow depth: 1.3 and 2.3 km; see section (d) of Table 3.

- Very low values of the double-couple percentage (DC%) that seem to be correlated in Table 3 with the polarity problems,
- Low values of the variance reduction (varred),
- Large departures of the MT-preferred depth from the location-derived depth,
- Small values of the min / max eigenvalue ratio (ill conditioning).

The overall behavior of the solutions is that when passing from the approach (a) to the approach (d), the number of problematic cases decreases (see the last column of Table 3). The approach (d) is considered the most reliable.

The MT solutions calculated for the source held fixed at hypocenter are more problematic than solutions with the grid-searched MT-optimized depth.

The MT solutions obtained from the depth grid search are mutually close for both the epicenters used (regional NOA or local CRL network). The only exception is Event 1 with the data problem.

Major discrepancies between MTs calculated with and without the depth grid search are related to the inaccurate location-derived depth (Event 2 and revision of Event 6).

A smooth and weak variation of the MT solution with the trial depth is by far not a sufficient criterion of its reliability; see, for example, stable (but incorrect) mechanisms at depth > 2.5 km in Figure 8.

The MT-preferred depths (and the corresponding MT solutions) are not free of problems. These depths and the corresponding MTs may be grossly wrong due to data errors. At the same time, the variance reduction can be quite large. Such a peculiar situation may be indicated by a big departure from the location-derived depth (Event 1).

The data errors (long-period disturbances, clipping) are dangerous because they are often masked by the band-pass filtration. If occurring at a near station, they result in an incorrect MT but large values of the variance reduction due to dominance of the near station.

Very near stations (distances less than 20 km) are highly problematic and, if possible, should not be used together with distant stations. Near stations with their large amplitudes have implicitly large weights in the least-squares inversion. The inversion tends to fit these stations well; the overall variance reduction is formally very large. However, data errors (see previous paragraphs) or small location errors easily destroy the inversion. The instability due to near station may be indicated by the low value of the min / max eigenvalue ratio (Event 4 prior revision).

Although all events were processed with apparently similar three-stations sets, some of the event-station configurations were actually much less convenient, as demonstrated by the varying values of the min / max eigenvalue ratio.

The variance reduction was not found to be correlated with magnitude.

A Note on the Magnitude and Moment

Comparing all moment magnitude determinations per event, they changed not more than 0.1 units for the revised solutions, except Event 1 (0.2 units). From a practical point of view, when comparing with standard magnitude variations for an event among different agencies, such a variation of M_w is small. From a scientific viewpoint, the 0.2 unit increase of M_w is equivalent to the seismic-moment increase by a factor of 2, which is not negligible. Moreover, prior to revision, the M_w change across approaches (a)–(d) amounted for 0.2 units (0.4 units for Event 1). We conclude that, although better than magnitude, the seismic moment is not as stable a parameter as often believed.

Three effects contribute to variability of the moment estimate for an event: imprecise waveform modeling, uncertain source depth, and uncertain crustal structure. Imprecise modeling, for example, when including higher frequencies, decreases the moment estimate because least-squares waveform inversions are characterized by proportionality between correlation and the synthetic data norm (hence moment). With regards to the depth, in two crustal models we obtain two estimates of the optimum depth, which may have a different shear-wave speed β and density ρ . Moment, being proportional to the product $\rho\beta^3$ at the source depth, is thus highly sensitive to the adopted crustal model. That is why a significantly more stable estimate of the source size would be provided by seismic potency, only proportional to β (Ben-Zion, 2001).

A Note on Independent Solutions

Two events (Events 5 and 6) were also processed by the Swiss Seismological Service (SED, ETH-Zurich; method in Braunmiller *et al.* [2002]). As shown in Table 4, the results are very close to those in Table 3. This comparison serves as an important check, because the methods are independent and complementary: many stations (17 and 30 stations for Event 5 and 6, respectively) at regional epicentral distances of the order of 1000 km, and periods > 30 sec on the side of SED, contrasting with fewer stations (three) at near distances < 100 km and periods around 10 sec in this article. It shows the capability of large continental networks to obtain moment-tensor solutions slightly below M_w 4.5 (Event 5) thanks to well-developed surface waves at larger distances in some cases. Simultaneously, it proves the capability of a few stations for a near-regional moment-tensor inversion, important mainly for weak events that are poorly recorded at larger distances. Calibration of the near-regional paths is also important for stronger events, allowing use of the periods as short as 10 sec (hard to model at larger distances in simple crustal models) to obtain insights into possible source complexities.

Conclusion

The article aimed at better understanding methodical problems of the moment-tensor (MT) calculation for weak events ($M_w \sim 4$) or lower. MTs of weak events are often determined by a single agency (network), thus lacking independent validation. We investigated how to increase reliability of the single-agency solutions through various multiple

checks. The article focused on the inversion of complete near-regional waveforms (in the range of 0.08–0.15 Hz, i.e., 6.7–12.5 sec) and discussed six representative $M \sim 4$ events in the Gulf of Corinth, Greece. Complete broadband waveforms were employed from several three-station sets at near-regional distances (8–103 km). We focused on one factor significantly affecting the MT, especially the assumed source position. The MTs were repeatedly calculated for two independent locations—from a regional and a local network. The source depth was held fixed at the hypocenter and was also grid searched to optimize the waveform match. The main results are in Table 3 and Figures 5 and 6. (See also the color versions of Figures 5 and 6, along with Figure S1, in the electronic edition of *BSSA*.)

Basically, the study consisted of two parts. The initial part resulted in a rather pessimistic indication that for some events (mainly Events 1 and 2), the MT solutions are unstable.

In the second part (additional beach balls for Events 1, 2, 4, and 6 in Fig. 5), the solutions were thoroughly revised and mostly stabilized. The problem of Event 1 was identified as due to an insufficient prior check of the data at the nearest station (a long-period disturbance). The problem of Event 2 was explained as related to its very shallow depth (of about 1–3 km), not detected during routine locations due to the inadequate shallow part of the crustal model. The problem of Event 4 was explained as due to a very small epicentral distance to the nearest station (8 km). The opposite problem, that is, a puzzling similarity of the repeated MT solutions of Event 6 for the dissimilar epicenter positions, was explained by the inadequacy of the crustal model used below Moho.

In general, an optimistic implication is that even a single agency can detect problematic MT solutions. As shown in the article, most important are the problem indicators, such as: (i) major problems of the first-motion polarities, often correlating with (ii) very low values of the double-couple percentage (DC%), (iii) large departures of the MT-preferred depth from the location-derived depth, and (iv) low values of the min / max eigenvalue ratio of the least-squares equations. It is always recommended to perform the MT inversion with a grid search below two alternative epicenters and to also add another indicator (v) a large difference between MT solutions for two close epicenters. Obviously, the optimum case is the absence of any problem indicator.

Less fortunate, but alarming, is the finding that some broadly used success indicators have a very limited value. For example, a large value of the overall variance reduction

Table 4
Solution of Two Events by an Independent Method*

Event Number	Longitude (°E)	Latitude (°N)	Depth (km)	Strike (°)	Dip (°)	Rake (°)	M_w
5	21.82	38.32	15	101	78	−29	4.2
6	22.73	38.26	102	117	45	−140	4.7

*SED (ETH Zurich) Regional Moment Tensor Catalogue; see Data and Resources section.

is not sufficient; incorrect MT solutions were demonstrated, characterized by large values of varred. Also, the popular stability of the MT solution with varying depth is nothing but a necessary condition for the MT reliability.

Practical recommendations for how to at least partially avoid problematic MT solutions are as follows. (1) The MT solutions for a single depth (hypocenter) are discouraged, even if we believe that the location is accurate enough; small formal location errors do not fully reveal inadequacy of the crustal model, thus leading to inadequacy of some locations. (2) The MT solutions with the grid-searched depth are encouraged because, in general, they tend to the correct depth. However, this is only true provided the data are free of problems (e.g., clipping). (3) Very near stations (distances less than 20 km) are highly problematic and, if possible, should not be used in the waveform inversion. Near stations with their large amplitudes have implicitly large weights in the least-squares inversion. The inversion tends to fit these stations well; the overall variance reduction is formally very large. Data errors, or small location errors, then easily bias the whole inversion. (5) If the MT-preferred depth strongly deviates from the location-derived depth (and, at the same time, we are sure about the data quality and problem is well conditioned), it is time to reconsider the location result. In particular, very shallow events can easily be mislocated deeper due to absence of a near station with *P* and *S* readings, and/or due to a crustal model inadequate at shallow depths.

Finally, the article clearly demonstrated how easily one might fall in various traps of the MT inversion. If a network massively reports fault-plane solutions of weak events calculated without enough care, inaccurate MT solutions represent nothing but an information noise, hardly usable to correctly derive the acting stress field. The only way towards fault-plane solutions truly reflecting small-scale tectonic features is through a very cautious processing of weak events, including not only the standard concern about the signal-to-noise ratio, proper frequency band, etc., but mainly the high-quality relocations and the (often overlooked) raw data-quality checks.

Data and Resources

Seismograms from the seismic stations SER and MAM were collected as part of the Prague–Patras project (<http://seis30.karlov.mff.cuni.cz/>); the data are available upon request. Seismograms from the other broadband stations used were collected by the Hellenic Seismological Broadband Network (HL) operated by the Institute of Geodynamics, National Observatory of Athens (NOA; <http://bbnet.gein.noa.gr/>); these data are available upon request. We used these data as a continuation of a preliminary study (Jansky *et al.*, 2006).

The preliminary locations were taken from public seismicity catalogs available at <http://www.gein.noa.gr/>.

The phase data from a local SP network were collected as part of the Corinth Rift Laboratory project (<http://consortium.ifp.fr/corinth/>) and are available upon request. The Regional Moment Tensor Catalogue of the Swiss Seismological Service, used for Table 4, is available at http://www.seismo.ethz.ch/moment_tensor/. The moment tensors were calculated using ISOLA software (Sokos and Zahradnik, 2008). This is free software that can be downloaded from the ISOLA web page (<http://seismo.geology.upatras.gr/isola/>).

Some plots were made using the Generic Mapping Tools version 4.2.1 of Wessel and Smith (1998) (www.soest.hawaii.edu/gmt/).

Acknowledgments

The work was financially supported by the European Commission Project Number 004043(GOCE)-3HAZ-CORINTH (coordinated by P. Bernard) and the following projects in the Czech Republic: GAUK 279/2006/B-GEOMFF, GACR 205/07/0502, and MSM0021620860.

References

- Adamova, P., E. Sokos, and J. Zahradnik (2008). Problematic non-double-couple mechanism of the 2002 Amfilochia M_w 5 earthquake, western Greece, *J. Seism.*, doi 10.1007/s10950-008-9112-4 (in press).
- Benetatos, Ch., A. Kiratzi, C. Papazachos, and G. Karakaisis (2004). Focal mechanisms of shallow and intermediate depth earthquakes along the Hellenic Arc, *J. Geodyn.* **37**, 253–296.
- Ben-Zion, Y. (2001). On quantification of the earthquake source, *Seism. Res. Lett.* **72**, 151–152.
- Bernard, P., H. Lyon-Caen, P. Briole, A. Deschamps, F. Boudin, K. Makropoulos, P. Papadimitriou, F. Lemeille, G. Patau, H. Billiris, D. Paradissis, K. Papazissi, H. Castarède, O. Charade, A. Necessian, A. Avallone, F. Pacchiani, J. Zahradnik, S. Sacks, and A. Linde (2006). Seismicity, deformation and seismic hazard in the western rift of Corinth: new insights from the Corinth Rift Laboratory (CRL), *Tectonophysics* **426**, 7–30.
- Bernardi, F., J. Braunmiller, U. Kradolfer, and D. Giardini (2004). Automatic regional moment tensor inversion in the European-Mediterranean region, *Geophys. J. Int.* **157**, 703–716.
- Braunmiller, J., U. Kradolfer, M. Baer, and D. Giardini (2002). Regional moment tensor determination in the European-Mediterranean area—initial results, *Tectonophysics* **356**, 5–22.
- Bouchon, M. (2003). A review of the discrete wavenumber method, *Pure Appl. Geophys.* **160**, 445–465.
- Campus, P., and D. Faeh (1997). Seismic monitoring of explosions: a method to extract information on the isotropic component of the seismic source, *J. Seismol.* **1**, 205–218.
- Campus, P., P. Suhadolc, G. E. Panza, and J. Sileny (1996). Complete moment tensor retrieval for weak events: application to orogenic and volcanic areas, *Tectonophysics* **261**, 147–163.
- Cervinkova, D. (2006). Study of source process of Greek earthquakes, *BS Thesis*, Charles University (in Czech).
- Cesca, S., E. Buforn, and T. Dahm (2006). Amplitude spectra moment tensor inversion of shallow earthquakes in Spain, *Geophys. J. Int.* **166**, 839–854.
- Clinton, J. F., E. Hauksson, and K. Solanki (2006). An evaluation of the SCSN moment tensor solutions: robustness of the M_w magnitude scale, style and automation of the method, *Bull. Seismol. Soc. Am.* **96**, 1689–1705.
- Coutant, O. (1990). Program of numerical simulation AXITRA, Laboratoire de Géophysique Interne et Tectonophysique Report, University of Joseph Fourier (in French).

- Dreger, D., and B. Savage (1999). Aftershocks of the 1952 Kern County, California, earthquake sequence, *Bull. Seismol. Soc. Am.* **89**, 1094–1108.
- Dreger, D., and B. Woods (2002). Regional distance seismic moment tensors of nuclear explosions, *Tectonophysics* **356**, 139–156.
- Frohlich, C. (1994). Earthquakes with non-double-couple mechanisms, *Science* **264**, 804–809.
- Haslinger, F., E. Kissling, J. Ansoerge, D. Hatzfeld, E. Papadimitriou, V. Karakostas, K. Makropoulos, H.-G. Kahle, and Y. Peter (1999). 3D crustal structure from local earthquake tomography around the Gulf of Arta (Ionian region, NW Greece), *Tectonophysics* **304**, 201–218.
- Henry, C., J. H. Woodhouse, and S. Das (2002). Stability of earthquake moment tensor inversions: effect of the double-couple constraint, *Tectonophysics* **356**, 115–124.
- Jansky, J., J. Zahradnik, O. Novotny, V. Plicka, and G. Stavrakakis (2006). Waveform inversion of M 4 events in the Gulf of Corinth—ID 1880, SC-A0 poster at the *First European Conference on Earthquake Engineering and Seismology*, 3–8 September 2006, Geneva, Switzerland, 274 (abstract book).
- Jechumtalova, Z., and J. Sileny (2005). Amplitude ratios for complete moment tensor retrieval, *Geophys. Res. Lett.* **32**, L22303.
- Jost, M. L., and R. B. Hermann (1989). A student's guide to and review of moment tensor, *Seism. Res. Lett.* **60**, 37–57.
- Jost, M. L., O. Knabenbauer, J. Cheng, and H.-P. Harjes (2002). Fault plane solutions of microearthquakes and small events in the Hellenic arc, *Tectonophysics* **356**, 87–114.
- Julian, B. R., A. D. Miller, and G. R. Foulger (1998). Non-double-couple earthquakes I. theory, *Rev. Geophys.* **36**, 525–549.
- Kikuchi, M., and H. Kanamori (1991). Inversion of complex body waves—III., *Bull. Seismol. Soc. Am.* **81**, 2335–2350.
- Latorre, D., J. Virieux, T. Monfret, V. Monteiller, T. Vanorio, J.-L. Got, and H. Lyon-Caen (2004). A new seismic tomography of Aigion area (Gulf of Corinth, Greece) from the 1991 data set, *Geophys. J. Int.* **159**, 1013–1031.
- Lyon-Caen, H., P. Papadimitriou, A. Deschamps, P. Bernard, K. Makropoulos, F. Pacchiani, and G. Patau (2004). First results of the CRLN seismic array in the western Corinth rift: evidence for old fault reactivation, *C. R. Geosci.* **336**, 343–351.
- Melis, N. S., and K. I. Konstantinou (2006). Real-time seismic monitoring in the Greek region: an example from the 17 October 2005 East Aegean Sea earthquake sequence, *Seism. Res. Lett.* **77**, 364–370.
- Novotny, O., J. Zahradnik, and G.-A. Tselentis (2001). North-western Turkey earthquakes and the crustal structure inferred from surface waves observed in the Corinth Gulf, Greece, *Bull. Seismol. Soc. Am.* **91**, 875–879.
- Pondrelli, S., S. Salimbeni, G. Ekström, A. Morelli, P. Gasperini, and G. Vannucci (2006). The Italian CMT dataset from 1977 to the present, *Phys. Earth Planet. Interiors* **159**, 286–303.
- Richardson, E., and T. H. Jordan (2002). Low-frequency properties of intermediate-focus earthquakes, *Bull. Seismol. Soc. Am.* **92**, 2434–2448.
- Rigo, A., H. Lyon-Caen, R. Armijo, A. Deschamps, D. Hatzfeld, K. Makropoulos, P. Papadimitriou, and I. Kassaras (1996). A microseismic study in the western part of the Gulf of Corinth (Greece): implications for large scale normal faulting mechanisms, *Geophys. J. Int.* **126**, 663–688.
- Roessler, D., F. Krueger, and G. Ruempker (2007). Inversion for seismic moment tensors in anisotropic media using standard techniques for isotropic media, *Geophys. J. Int.* **169**, 136–148.
- Sileny, J., and A. Milev (2006). Seismic moment tensor resolution on a local scale: simulated rockburst and mine-induced seismic events in the Kopanang gold mine, South Africa, *Pure Appl. Geophys.* **163**, 1495–1513.
- Sileny, J., P. Campus, and G. F. Panza (1996). Seismic moment tensor resolution by waveform inversion of a few local noisy records—I. synthetic tests, *Geophys. J. Int.* **126**, 605–619.
- Sokos, E., and J. Zahradnik (2008). ISOLA—a Fortran code and a Matlab GUI to perform multiple-point source inversion of seismic data, *Comput. Geosci.* **34**, 967–977.
- Somerville, P., K. Irikura, R. Graves, S. Sawada, D. Wald, N. Abrahamson, Y. Iwasaki, T. Kagawa, N. Smith, and A. Kowada (1999). Characterizing crustal earthquake slip models for the prediction of strong ground motion, *Seism. Res. Lett.* **70**, 59–80.
- Tajima, F., Ch. Mégnin, D. S. Dreger, and B. Romanowicz (2002). Feasibility of real-time broadband waveform inversion for simultaneous moment tensor and centroid location determination, *Bull. Seismol. Soc. Am.* **92**, 739–750.
- Templeton, D. C., and D. S. Dreger (2006). Non-double-couple earthquakes in the Long Valley volcanic region, *Bull. Seismol. Soc. Am.* **96**, 69–79.
- Tselentis, G.-A., N. S. Melis, E. Sokos, and K. Papatsimpa (1996). The Egeion June 15, 1995 (6.2 M_L) earthquake, Western Greece, *Pure Appl. Geophys.* **147**, 83–98.
- Vavrycuk, V. (2007). On the retrieval of moment tensors from borehole data, *Geophys. Prospect.* **55**, 381–391.
- Wessel, P., and W. H. F. Smith (1998). New improved version of the Generic Mapping Tools released, *Eos Trans. AGU* **79**, 579.
- Yunga, S., A. Lutikov, and O. Molchanov (2005). Non-double-couple seismic sources, faults interaction and hypothesis of self-organized criticality, *Nat. Hazards Earth Syst. Sci.* **5**, 11–15.
- Zahradnik, J. (2004). How many stations do we need to record ground motion at a station?, *Studia Geophys. Geodyn.* **48**, 483–492.
- Zahradnik, J., and A. Plesinger (2005). Long-period pulses in broadband records of near earthquakes, *Bull. Seismol. Soc. Am.* **95**, 1928–1939.
- Zahradnik, J., A. Serpetsidaki, E. Sokos, and G.-A. Tselentis (2005). Iterative deconvolution of regional waveforms and double-event interpretation of the 2003 Lefkada earthquake, Greece, *Bull. Seismol. Soc. Am.* **95**, 159–172.
- Zahradnik, J., E. Sokos, G.-A. Tselentis, and N. Martakis (2008). Non-double-couple mechanism of moderate earthquakes near Zakynthos, Greece, April 2006; explanation in terms of complexity, *Geophys. Prospect.* **56**, 341–356.
- Zahradnik, J., F. Gallovic, E. Sokos, A. Serpetsidaki, and G.-A. Tselentis (2008). Quick fault-plane identification by a geometrical method: application to the M_w 6.2 Leonidio earthquake, January 6, 2008, Greece, *Seism. Res. Lett.* **79**, 653–662.

Charles University in Prague
Faculty of Mathematics and Physics
Department of Geophysics
V Holesovickach 2
180 00 Prague, Czech Republic
Jiri.Zahradnik@mff.cuni.cz